

Feasible and simple preparation of Pd (II), Ni (II), and Pt (IV) complexes: Their biological and industrial applications and investigation of Pd (II) complex in Suzuki reaction

Eman khalil Ibrahim^{1*} , Jinan M.M.Al-Zinkee², Amer J. Jarad³

¹Ministry of Education, Diyala Education Directorate, Iraq.

²Department of Chemistry, College of Science, University of Diyala, Iraq.

³Department of Chemistry, College of Education for Pure Science /Ibn-Al-Haitham, University of Baghdad, Iraq.

*Corresponding author: scichemms2218@uodiyala.edu.iq

Review Paper

Received:

15 March 2024

Revised:

01 May 2024

Accepted:

08 May 2024

Published online:

15 June 2024

© The Author(s) 2024

Abstract:

A novel ligand, (E)-5-((2-hydroxy-4,6-dimethylphenyl)diazonyl)-2,3-dihydrophthalazine-1,4-dione, was synthesized through the reaction of 3,5-dimethylphenol with the diazonium salt of 5-amino-2,3-dihydrophthalazine-1,4-dione. The ligand underwent characterization through the utilization of diverse spectroscopic methods, including UV-Vis, FT-IR, ¹³C, and ¹H-NMR, alongside Mass spectroscopy and micro elemental analysis (Carbon, Hydrogen, Nitrogen, and Oxygen). Metal chelates of transition metals were prepared and analyzed using elemental analysis, mass spectra, atomic absorption, UV-Vis, FT-IR spectral analysis, as well as conductivity and magnetic measurements. The investigation into the compounds' nature was conducted by utilizing mole ratio and continuous contrast methods, where Beer's law was adhered to over a concentration range of 1×10^{-4} - 3×10^{-4} mol/L. The determination of the molar absorptivity of the compound solutions was carried out. Analytical data analysis indicated that all complexes demonstrated a metal-ligand ratio of 1:2, with the exception of the palladium complex, which exhibited a 1:1 ratio. Physicochemical data indicated an octahedral structure for the Pt (IV) and Ni (II) complexes and a square planar structure for the Pd (II) complex. The Pd complex was utilized in a carbon-carbon Suzuki coupling reaction to evaluate the application of this complex. Furthermore, the biological activity of these complexes was assessed on the proliferation of human blood lymphocytes. The results demonstrated that the ligand inhibited cell division at varying levels, with the inhibition increasing with higher concentrations. Furthermore, the Pd complex caused a prolonged arrest during mitosis at the boundary between metaphase and anaphase, leading to the suppression of proliferation in the lymphocyte cell line. The stability of the dyes was assessed in terms of light exposure and resistance to detergents.

Keywords: Metal chelates; Azo dyes; Microbial studies; Luminol derivatives; Suzuki reaction; Catalyst

1. Introduction

Azo dyes have been recognized as a highly innovative and significant group within organic compounds, finding numerous scientific and industrial uses [1]. Due to their vibrant colors, azo dyes are extensively utilized in

liquid crystal display color filters [2], lasers, nonlinear optics, photovoltaic production [3], chemical sensors, pharmaceuticals, cosmetics, food products, and various organic syntheses [4]. Recently, azo dyes have also been employed as corrosion inhibitors [5, 6]. In various fields,

azo dyes have demonstrated their potential and importance, known for their stability, sensitivity, and proficiency in coordination chemistry [7]. Metal ion complexes with azo ligands have resulted in a broad spectrum of varied and essential uses in scientific investigations [8]. This metal chelates have garnered significant attention due to their roles in biology, medicine, and industry, as they possess the ability to mimic complex molecules involved in essential biological processes like oxygen transport, electron transfer, and catalysis [9, 10]. Furthermore, metal chelates have been extensively studied and admired for their intriguing electronic and geometrical properties, which have implications across various fields of application [11–13].

The field of chemical industry has experienced substantial effects from palladium-catalyzed cross-coupling reactions, which include the Heck, Stille, Negishi, Kumada, and Hiyama reactions [14–17]. The involvement of these responses has been crucial in the creation of a wide range of natural substances, and agricultural chemicals, and in the fields of medicine and supramolecular chemistry. The Suzuki reaction is widely recognized as a highly efficient cross-coupling method for synthesizing unsymmetric biaryls Ar-Ar from arylboronic acids Ar-B(OH)₂ and aryl halides Ar-X (X= Cl, Br, I) among various other available methods [18–22]. The Suzuki reaction has garnered significant attention in the realm of organic chemistry owing to its operational simplicity, remarkable tolerance towards functional groups, and the environmentally benign nature of its initial constituents. The investigation of this specific reaction has garnered heightened attention due to these factors. The Suzuki cross-coupling reaction commonly utilizes a palladium catalyst that incorporates meticulously crafted ligands derived from phosphine. These ligands play a crucial role in enhancing the efficiency of the transformation process. However, phosphine ligands have certain drawbacks, including sensitivity to air and/or moisture, high cost, and toxicity. In recent years, there has been a significant focus on developing palladium catalysts that utilize more cost-effective phosphine-free ligands such as N-heterocyclic carbene [23], imidazole, thiol, anionic carbocyclic, carbocyclic, and porphyrin ligands. Azo

ligands, which fall under the category of phosphine-free ligands, have gained recognition for their effectiveness and suitability as organ catalyst ligands for palladium compounds. This recognition is due to their straightforward synthesis, lack of toxicity, and the adaptability of their steric and electronic characteristics.

Azo compounds containing a heterocyclic moiety have been significantly influential in the advancement of azo coordination compounds over the last fifty years [24]. This is due to their remarkable contributions in various areas such as medicinal, biological, analytical, and industrial research, attributed to their extensive conjugation and readily available lone pair of electrons [25]. The azo compounds and their metal complexes have been extensively researched due to their antioxidant and antimicrobial properties [26]. Heterocyclic azo derivatives are widely recognized for their pharmaceutical value and are commonly used as antibacterial, antineoplastics, antidiabetics, antitumor drugs, antituberculosis agents, and antiseptics. Moreover, they are renowned for their involvement in diverse biological reactions. For instance, the antibacterial and antifungal activities of 3-aryl-azo-4-hydroxy coumarin and its Ni (II) and Co (II) metal complexes were found to be remarkably effective [27]. The azo derivatives based on phenazone exhibited remarkable efficacy against both Gram-negative and Gram-positive bacteria when coordinated with Ni (II) and Cu (II) metal complexes, surpassing the activity of the unbound ligands.

The aim of this study is to create and synthesize azo compounds, as well as their complexes with Ni (II), Pd (II), and Pt (IV), using (E)-5-((2-hydroxy-4,6-dimethylphenyl)diazenyl)-2,3-dihydrophthalazine-1,4-dione as the starting material. These compounds will be analyzed using various physico-chemical techniques to determine their properties. Certainly, the fields of chemistry, biomedicine, and industry are undeniably influenced by the contributions of applied sciences. The chemical structure of the metal complexes that were prepared is illustrated in Fig. 1.

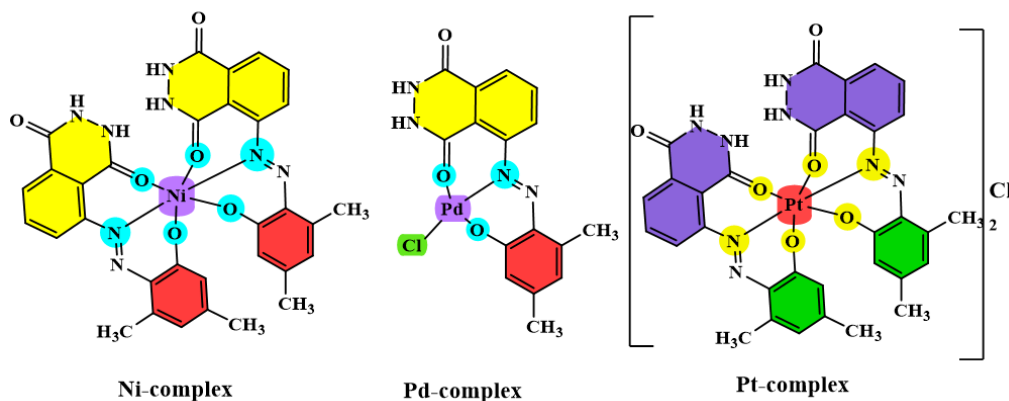


Figure 1. The chemical structure of prepared metal complexes.

2. Experimental

2.1 General methods

The chemicals utilized for collection purposes included NiCl₂.6H₂O, PdCl₂, and H₂PtCl₆.6H₂O from Merck, as well as 3,5-dimethylphenol and 5-amino-2,3-dihydrophthalazine-1,4-dione from B.D.H. In the laboratory of Agilent Technologies at the University of Tehran in Iran, a Bruker-400 MHz Ultra Shield spectrometer was used to obtain ¹³C and ¹H-NMR spectra. Dimethylsulfoxide was employed as the solvent, while tetramethylsaline served as the reference compound. The conductivity of the compounds dissolved in ethyl alcohol (10⁻³ M/L) was measured at 25 °C using a Philips PW-Digital Conductance meter. For micro elemental analysis (C, H, N, O), Euro vector EA 3000, single V.3.O. was utilized. The magnetic characteristics were refined by applying the Auto Magnetic Susceptibility at 25 °C using Sherwood equipment. Atomic absorbance was measured using a Shimadzu A. A-160A Atomic Absorption/Flame Emission Spectrophotometer, while a UV-Vis-160A spectrophotometer was employed to record the UV-visible spectrum. The infrared spectrum was created using KBr disks and analyzed using a Shimadzu FTIR-8400S Fourier Transform Infrared Spectrophotometer within the range of 4000-400 cm⁻¹. Mass spectrometry measurements were conducted using a Shimadzu (E170-EV) Spectrometer. Furthermore, the utilization of the Stuart Melting Point Apparatus facilitated the determination of the melting points of the compounds.

2.2 Preparation of azo ligand

The compound 5-amino-2,3-dihydrophthalazine-1,4-dione (0.442 g, 1 mmol) was heated in a mixture of 10 mL ethanol and 2 mL concentrated hydrochloric acid (HCl) [28]. The resultant solution was subsequently diazotized at a temperature of 5 °C utilizing a 10% (NaNO₂) solution. The chilled ethanolic solution of 3,5-dimethylphenol (0.305 g, 1 mmol) was carefully mixed with the diazotized solution, which was added dropwise with agitation. Subsequently, an azo ligand precipitate was formed by introducing a 25 mL solution of 1 M sodium hydroxide (NaOH) into the dark-colored mixture. The precipitate was subsequently filtered and washed using a solution composed of equal parts ethanol (C₂H₅OH) and water (H₂O). Finally, the resulting filtrate was left to dry naturally.

2.3 Preparation of buffer solution

In a volume of one liter, ammonium acetate (0.01M, 0.771 gram) was dissolved in doubly deionized water. The pH range necessitated the utilization of CH₃COOH or NH₃ solutions in order to maintain it within the range of 5 to 9.

2.4 Preparation of standard solution

Mineral salt buffer solutions in a range between focus (10⁻⁵-10⁻³ M/L) were generated at pH (5-9). A significant volume of ethanolic ligand solutions with concentrations between (10⁻⁵-10⁻³) M/L were created at the same time.

2.5 Preparation of metal complexes

The ligand solution (0.310 g, 2 mmol) in ethanol was slowly added while stirring to separate solutions of NiCl₂.6H₂O (0.118 g), PdCl₂ (0.117 g), and H₂PtCl₆.6H₂O (0.259 g) dissolved in a buffer solution at pH 7. The mixture that ensued was allowed to cool until a precipitate with a dark hue appeared, following which it was filtered and subsequently rinsed multiple times using a solution consisting of water and ethanol in a 1:1 ratio.

2.6 The General approach for the Suzuki coupling reaction in the presence of Pd-complex

A mixture was prepared by combining Aryl halide (1.0 mmol), phenylboronic acid derivatives (1.1 mmol), Pd-complex (30 mg), K₂CO₃ (1.5 mmol), and H₂O: EtOH (2:1) (3.0 mL) in a 25 mL round-bottom-flask equipped with a condenser and a magnetic stirring bar. The mixture was subsequently heated to 80 °C while being continuously monitored via TLC until the aryl halide was completely converted. After the reaction was finished, 5.0 mL of hot water and 5.0 mL of ethyl acetate were added to the reaction mixture. The Pd-complex catalyst was obtained by subjecting it to reduced pressure using a vacuum pump via sintered-glass grade-4. The crude product was obtained by concentrating the resulting organic solution with a rotary evaporator. Various purification techniques were subsequently employed to refine each of the synthesized compounds.

2.7 Biological part

The impact of the ligand and its complexes on lymphatic cell division in human blood was investigated through short-term culture, following the methodology outlined by Verma and Babu. Blood samples were collected randomly from individuals of varying ages using a medical syringe containing 5 mL of heparin solution per person for subsequent testing [29].

2.8 Transplantation of Blood and prepared compound

The compound was introduced into the prepared culture tubes, each at concentrations of 25, 50, and 100 mg/mL, along with the complete RPMI-1640 culture medium. The concentration of each sample was replicated three times, and the resulting mixture was then adjusted to a final volume of 5 mL. Afterward, a 5 mL syringe was utilized to dispense 0.5 mL of blood into each tube. Subsequently, 0.1 mL of the lymphocyte-cleaving agent (PHA) was added to the medium and gently mixed. The tubes were subsequently placed in an incubator set at 37 °C on a platform that was tilted and were mixed every 12 hours. Another group of tubes was labeled as controls, where no extra extract was included.

2.9 Harvesting of Cell

In the experimental setup, a precise amount of 0.1 mL of colchicine was added to the control tube. This colchicine was present at a concentration of 10 mg/mL and was introduced exactly 15 minutes prior to the completion of the initial culture period. Conversely, the treated tubes did not receive any colchicine. Subsequently, all tubes were placed

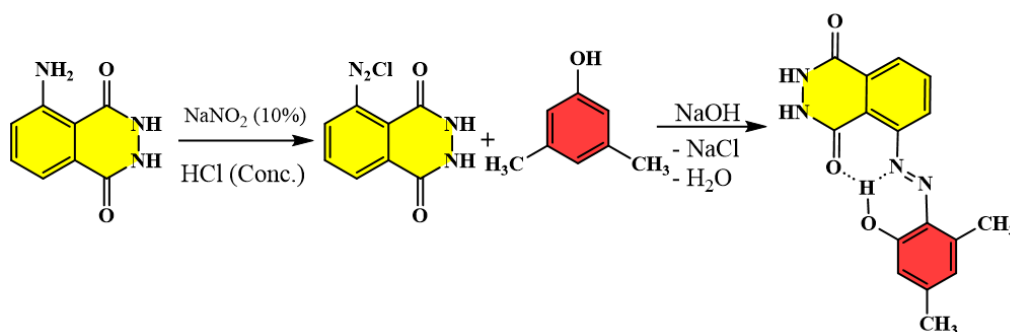
back into the incubator. After the period of incubation, centrifugation was performed on all tubes at a velocity of 1500 revolutions per minute for a duration of 10 minutes. The resulting liquid was discarded, while the precipitate was thoroughly mixed with the remaining culture medium. The tubes were each slowly treated with a hypotonic solution of 0.075 M, varying in volume from 5 to 10 mL. The tubes were carefully heated and agitated at a temperature of 37 °C by immersing them in a water bath for a period of 30 minutes. Subsequently, the tubes underwent another round of centrifugation at a speed of 1500 rpm for a duration of 10 minutes, following which the resultant liquid was disposed of.

2.10 Fixation, Washing, Dropping, Pigmentation, microscopy, and Mitotic Index

The precipitate was subjected to extensive agitation, after which a small amount of cold Fixative was added to the inner surface of the tube while maintaining continuous shaking. The volume was then adjusted to 5ml. Following this, the specimens were blended utilizing a Vortex mixer, and then the containers were stored in a refrigerated environment at 4 degrees Celsius for a duration of 30 minutes. Subsequently, the tubes underwent centrifugation at a speed of 1500 revolutions per minute for a duration of 10 minutes, resulting in the separation of the filtrate and the retention of the precipitated cells. The fixation process was reiterated until the suspension displayed a clear color. The precipitate was re-suspended by introducing 1ml of the fixative and stored at -20 °C. Clean, cool, wet, and fat-free glass slides were readied, and the cells were thoroughly mixed before being dropped onto the cold slides using a Pasteur pipette from a distance of 0.5-1 m, allowing them to dry. Finally, the slides were stained with a prepared Giemsa stain diluted with warm Sorensen buffer solution at a ratio of 4:1 for 2-3 minutes, washed with Sorensen buffer, left to dry, and examined under light microscopy to determine the Mitotic Index (ML). The total number of cells examined (1000) was used to divide the cells in metaphase, as described.

Mitotic index (ML %) :

$$\frac{\text{The number of dividing cells}}{\text{The total number of cells is 1000}} \times 100$$



Scheme 1. Synthesis of azo ligand.

2.11 Dyeing process

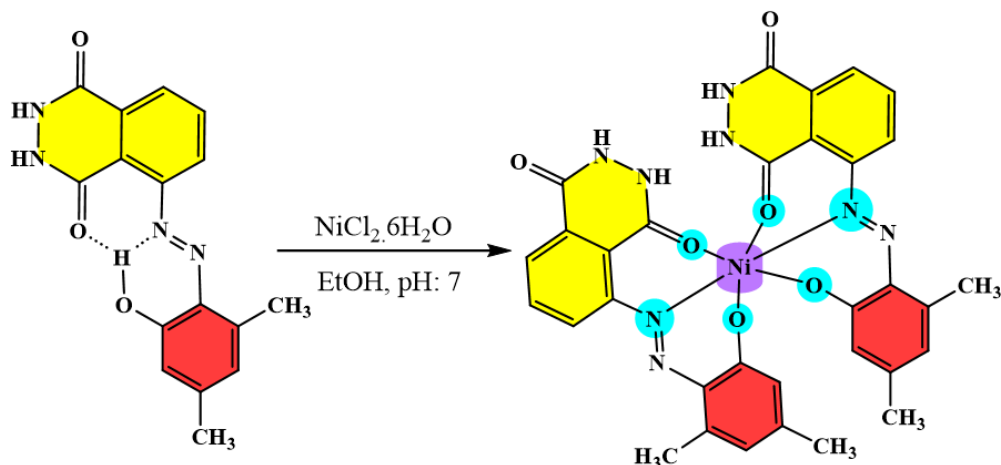
The chemicals are produced and applied via cotton fibers as (1% shade) offers dyeing qualities. The tissue dyeing continues for one hour at (15–20 °C) and a pH of (10).

3. Results and discussion

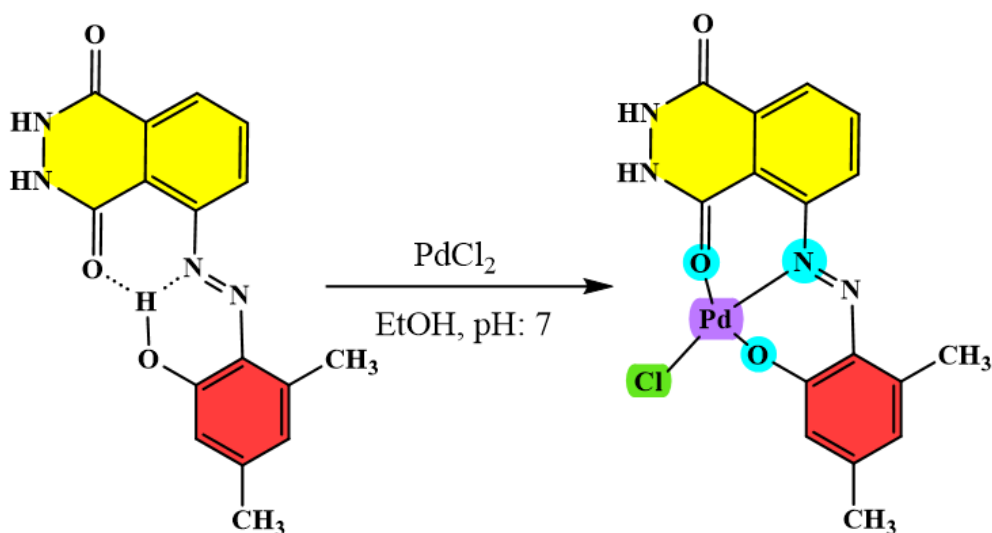
3.1 Preparation and characterization of ligand and metal complexes

Scheme 1 demonstrated the procedure for synthesizing the azo ligand. At first, the compound 5-amino-2,3-dihydrophthalazine-1,4-dione was liquefied within a solution comprising 10 mL of ethanol and 2 mL of concentrated hydrochloric acid (HCl). The solution obtained was subsequently exposed to diazotization at a temperature of 5 °C by utilizing a 10% sodium nitrite (NaNO₂) solution. Following this, the solution containing the diazotized compound was carefully introduced into a chilled ethanolic solution of 3,5-dimethylphenol while stirring. Following this, a 25 mL solution of sodium hydroxide (NaOH) with a concentration of 1 M was introduced to the mixture, resulting in the precipitation of the azo ligand. The solid was filtered afterwards and washed with a solution composed of ethanol (C₂H₅OH) and water (H₂O) in a 1:1 ratio. Finally, the filtered product was left to dry. To confirm the identity of the prepared ligand, various spectral studies including ¹H and ¹³C-NMR, Mass, FT-IR, and UV-Vis were conducted, along with micro elemental analysis (C, H, N, O). The prepared aqueous-ethanol solutions were consistently utilized in order to examine the interaction between the metal salts and the synthesized ligand. Furthermore, for the synthesis of metal complexes (Schemes 2-4), the ligand solution in ethanol was slowly added, while stirring, to separate solutions of NiCl₂·6H₂O, PdCl₂, and H₂PtCl₆·6H₂O dissolved in a buffer solution at pH 7. The resultant blend was allowed to cool until a dark-hued sediment appeared, subsequently undergoing filtration and undergoing several washes with a 1:1 solution of water and ethanol. All of the metal complexes were characterized using FT-IR, NMR, Mass, and Uv-Vis's spectroscopy.

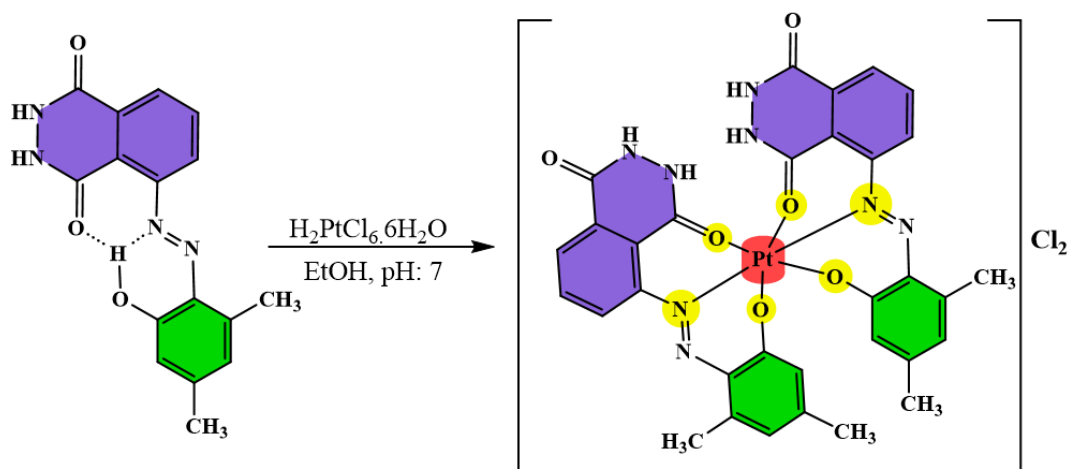
The ¹HNMR spectrum of the ligand (Fig. 2) shows several signals between δ=7.25-8.35 ppm, which have been designated as aromatic protons [30]. Furthermore, phthalazine exhibits signals at δ=10.55 ppm, representing the δ (NH) resonance, while phenol displays a signal at δ=10.15 ppm,



Scheme 2. Synthesis of Ni (II) complex.



Scheme 3. Synthesis of Pd (II) complex.



Scheme 4. Synthesis of Pt (IV) complex.

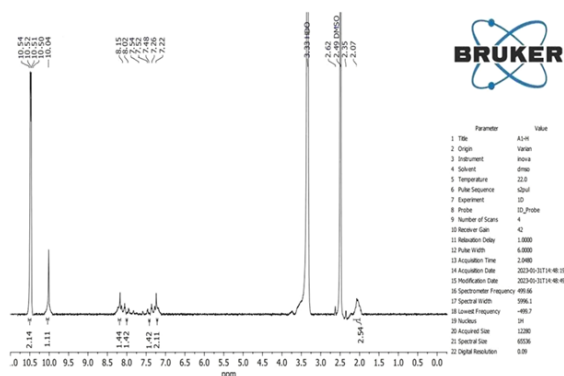


Figure 2. ^1H NMR spectrum of synthesized ligand.

corresponding to the δ (OH) resonance. The signals detected at a chemical shift of $\delta=3.35$ ppm and $\delta=2.49$ ppm are assigned to water and DMSO- d_6 , respectively [31, 32]. In addition, the signal at ($\delta=2.07$) ppm describes to δ (CH_3) of ligands.

Resonances at $\delta=30.02$ ppm and $\delta=35.02$ ppm were detected in the ^{13}C NMR spectrum of the ligand, indicating the presence of carbon atoms from the (CH_3) group in the phenol ring. Furthermore, various signals at $\delta=180.99$, 177.24, 172.45, 168.51, 162.91, 156.86, 154.20, 148.89, 145.97, and 137.44 ppm are indicative of the carbon atoms in the aromatic rings. The peaks observed at $\delta=205.20$ ppm and $\delta=185.20$ ppm are attributed to the carbon nuclei of the ($\text{C}=\text{O}$) and ($\text{C}-\text{OH}$) functional groups, respectively. Finally, the peak observed at a chemical shift of $\delta=40.30$ ppm can

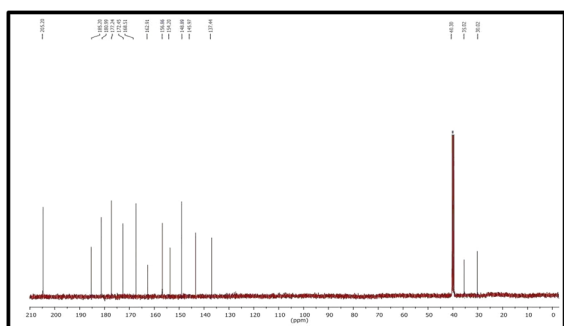


Figure 3. ^{13}C NMR spectrum of the synthesized ligand.

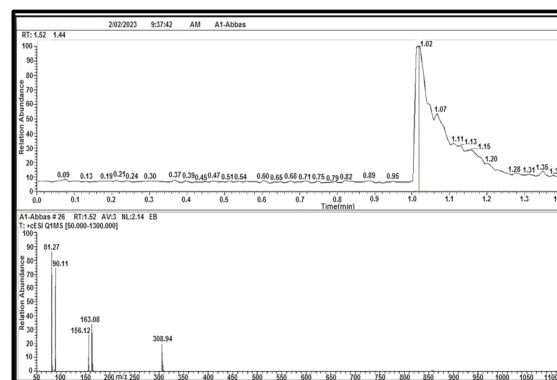


Figure 4. Mass spectrum of prepared ligand.

be assigned to DMSO- d_6 , as depicted in Fig. 3.

The ligand that was prepared exhibited a peak in its mass spectrum at $m/z = 308$, indicating the presence of the $\text{C}_{16}\text{H}_{12}\text{N}_4\text{O}_3^+$ formula (Fig. 4). The fragmentation patterns of the ligand are summarized in Scheme 5. Concerning the complexes, their mass spectrometry data revealed peaks with m/z values of 677, 450.5, and 813, which corresponded to the molecular formulas $\text{C}_{32}\text{H}_{26}\text{N}_8\text{O}_6\text{Ni}$, $\text{C}_{16}\text{H}_{13}\text{N}_4\text{O}_3\text{ClPd}$, and $[\text{C}_{32}\text{H}_{26}\text{N}_8\text{O}_6\text{Pt}]^{2+}$, respectively. The fragmentation patterns of the complexes are summarized in Schemes 6-8 and Figs. 5-7.

The synthesized ligands and metal complexes were analyzed for their physical properties such as color, melting point, and elemental composition. These findings were then organized and presented in Table 1.

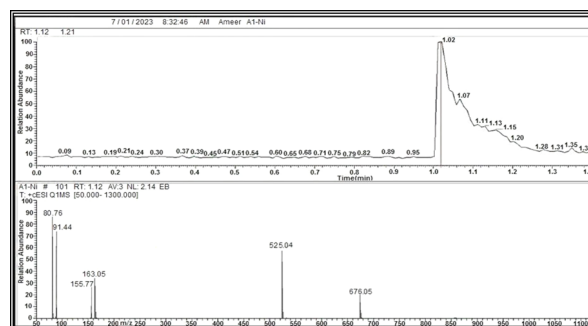
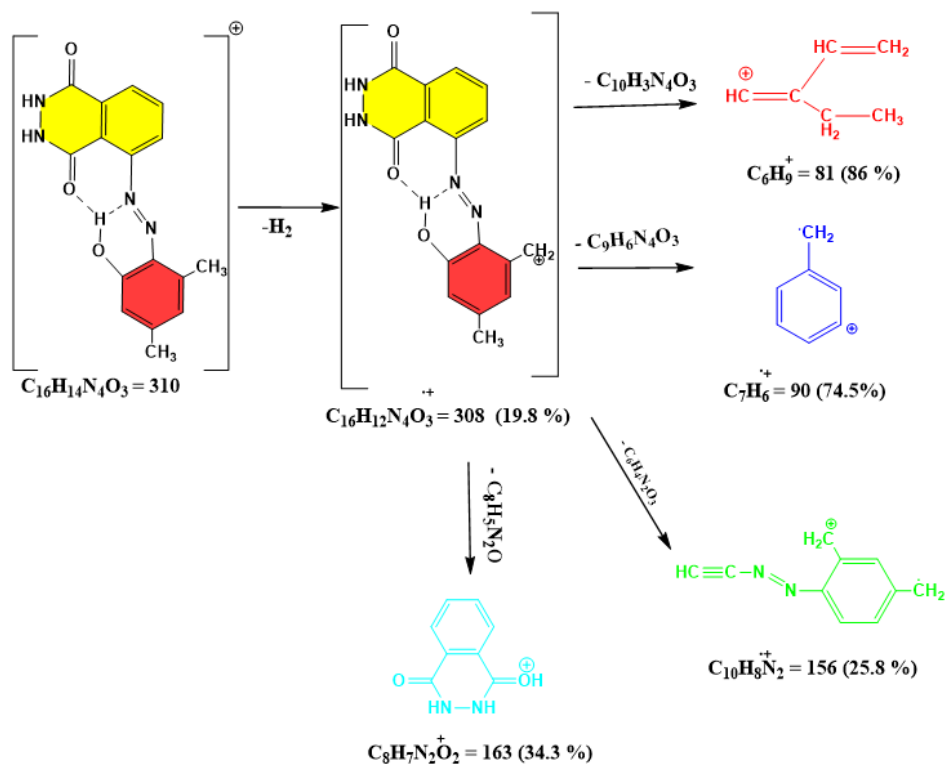


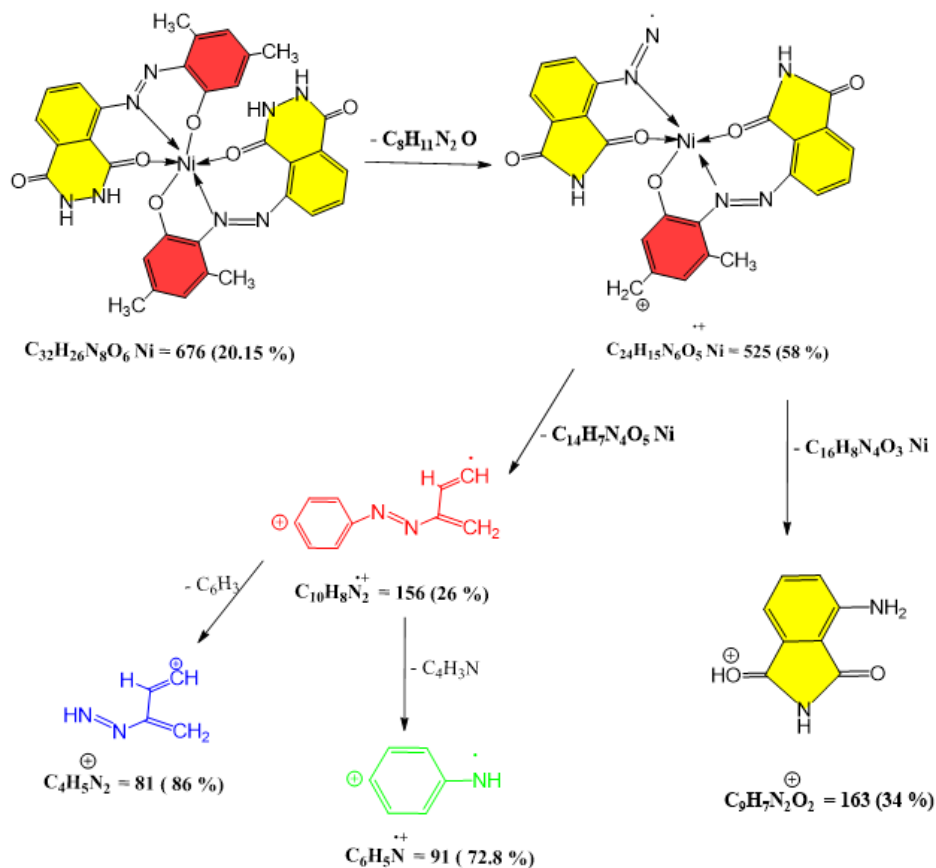
Figure 5. Mass spectrum of Ni (II) complex.

Table 1. Physical properties of the ligand and metal complexes.

compounds	color	M.P °C	yield (%)	analysis calc. (found)				
				M%	C%	H%	N%	O%
Ligand(L)	orange	258-260	81	-	61.93 (60.45)	4.51 (3.11)	18.06 (19.97)	15.48 (16.27)
$[\text{Ni}(\text{L})_2]$	dark orange	285-287	85	8.57 (7.87)	56.80 (55.98)	3.84 (2.87)	16.56 (15.77)	14.57 (14.04)
$[\text{Pd}(\text{L})\text{Cl}]$	brown	>300	84	23.53 (22.78)	42.61 (41.77)	2.88 (1.92)	12.43 (11.76)	10.65 (9.98)
$[\text{Pt}(\text{L})_2]\text{Cl}_2$	light brown	242 D	81	22.17 (21.93)	43.43 (42.85)	2.94 (2.03)	12.66 (11.85)	10.85 (9.82)



Scheme 5. Fragmentation pattern of synthesized ligand.



Scheme 6. Fragmentation pattern of Ni (II) complex.

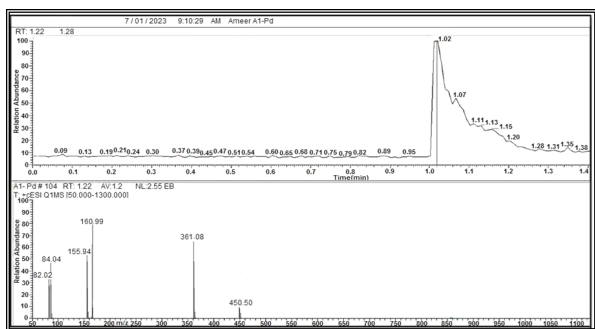


Figure 6. Mass spectrum of Pd (II) complex.

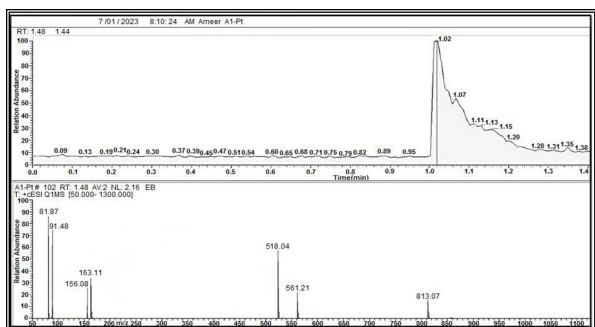


Figure 7. Mass spectrum of Pt (IV) complex.

3.2 Calibration curve

Within the range of molar concentrations (10^{-5} - 10^{-3} M/L) encompassing both aqueous ethyl alcohol ligand and metal ions, only a limited proportion (10^{-3} - 10^{-4} M/L) demonstrated adherence to Beer's law and displayed a discernible vivid hue. The correlation factor $R > 0.998$, as depicted in Fig. 8, further confirms the accuracy of the chosen straight lines, ensuring the selection of the most appropriate and optimal lines.

3.3 Model conditions

Upon manufacturing compounds, the initial step involves examining the interactions between the synthesized ligand and the less-studied metal ions. This is achieved by creating a spectrum through the combination of ligand and metal ion solutions to achieve a specific pH level, concentration, and a consistent maximum wavelength. The ratio of metal to ligand (M: L) is also established within the synthesized molecules. Subsequently, the solution that exhibits the high-

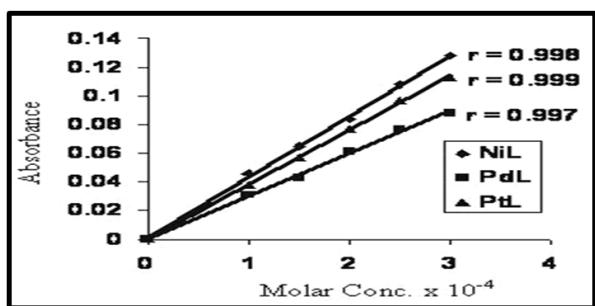


Figure 8. Linear relationship between absorption and molar condensation for three complexes.

est absorption at a consistent wavelength under varying pH conditions is identified as the optimal concentration. The results of this process are detailed in Table 3. The experiment further investigates the absorbance of all synthesized compounds in a buffer solution of $\text{NH}_4\text{OOCCH}_3$ within a pH range of 5 to 9. As illustrated in Fig. 9, each compound produced maintains the appropriate pH level.

3.4 Metal to ligand ratio

The utilization of mole ratio techniques has been implemented to ascertain the composition of complexes in solutions. The outcomes in both scenarios indicated a 1:2 ratio (metal to ligand) for the majority of complexes, except for Pd (II) which displayed a 1:1 ratio, as illustrated in Fig. 10. Table 2 provides a summary of the obtained outcomes and offers insights into the synthesis of these compounds.

3.5 The effect of time

The reaction concluded in a time frame of 5 minutes. The temperature was set at 25°C and subsequently held constant for approximately 90 minutes, attributed to the robust coordination of bonds with metal-salts. The findings are illustrated in Fig. 11.

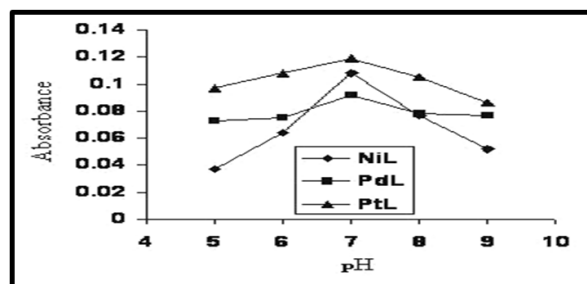


Figure 9. Effect of pH at absorption (λ_{max}) to the metal complexes.

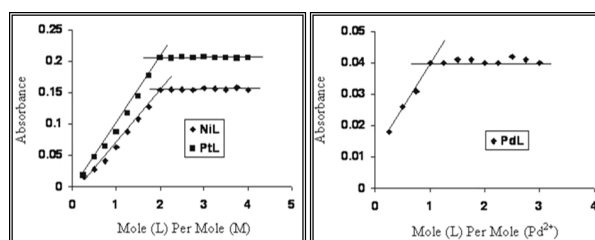


Figure 10. Mole ratio for the compound solutions.

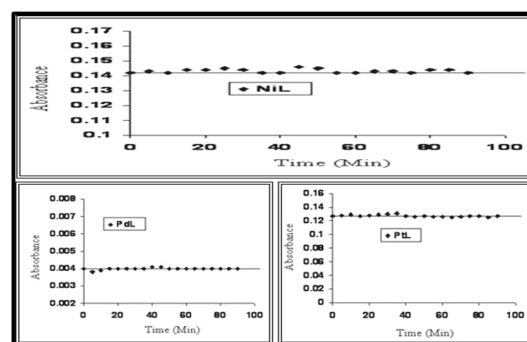


Figure 11. Effect of time on the produced compounds.

3.6 Gibbs free energy and Stability constant

The stability constant for the (1:2) metal to-ligand compound can be calculated using the following formulas:

$$K = \frac{1 - \alpha}{4\alpha^3 C^2}; \quad \alpha = \frac{A_m - A_s}{A_m} \quad (1)$$

While the ratio (1:1, M: L) calculated according to the equation:

$$K = 1 - \alpha/\alpha^2 c \quad (2)$$

The factors that should be taken into consideration include the degree of dissociation (α), the condensation to the compound solution (c) in mole/L, the absorption in a solution

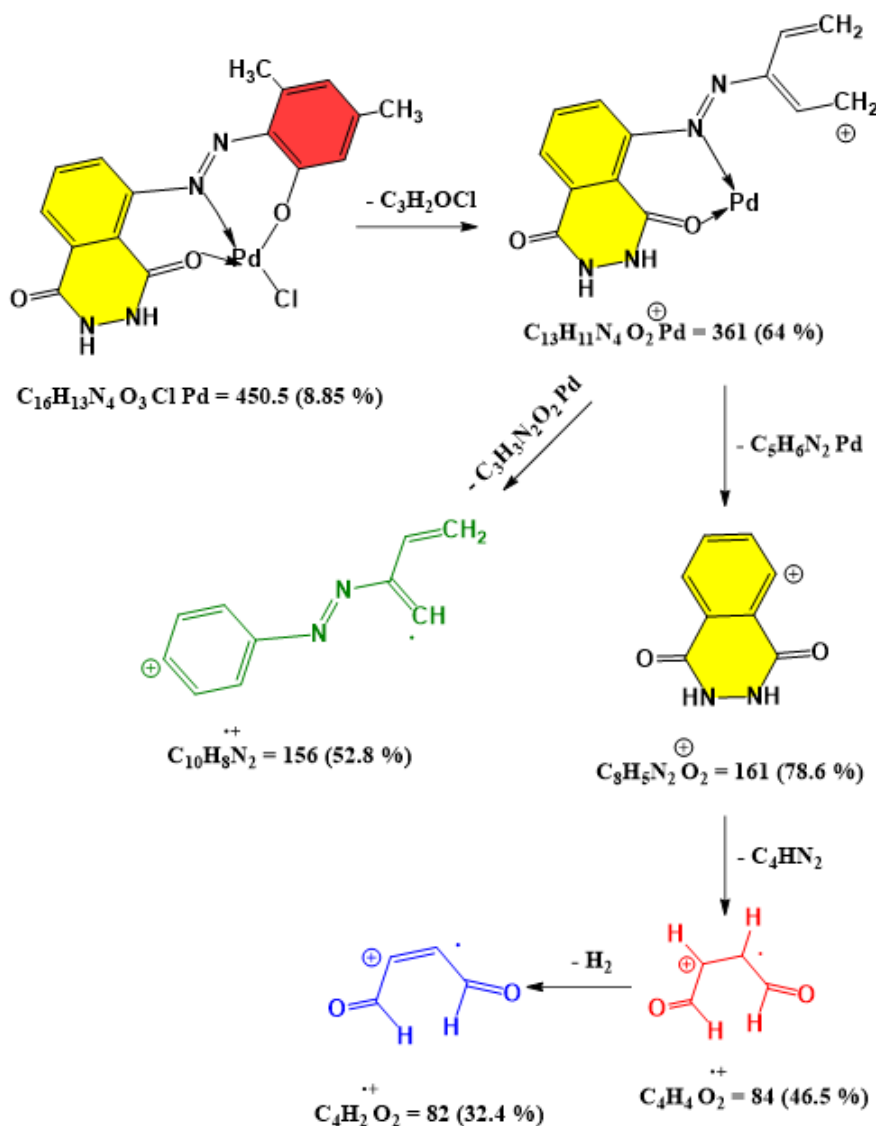
containing equal amounts of ligand and metal ion (A_s), and the absorption of a solution containing equal quantities of metal and excess ligand (A_m) [33]. High values of the equilibrium constant (K) are indicative of the significant stability exhibited by the formed complexes. Furthermore, a particular equation has been employed to examine the thermodynamic properties of Gibbs free energy (ΔG) [34].

$$\Delta G = -RT \ln k \quad (3)$$

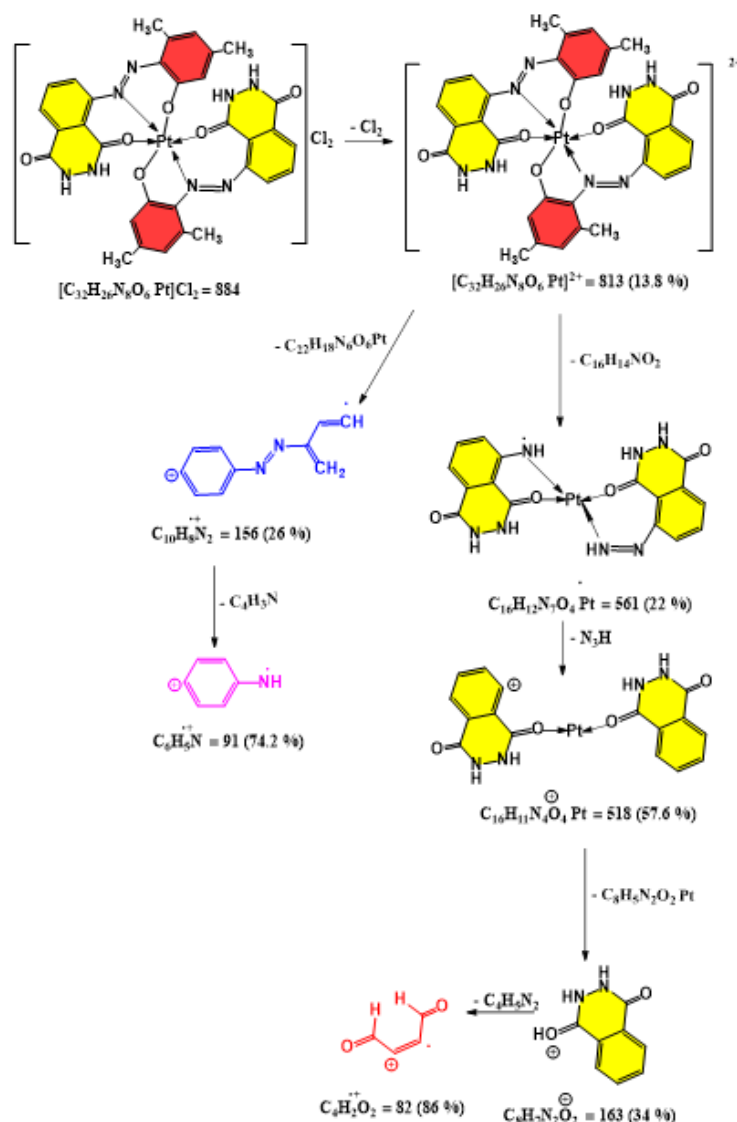
In Table 2, the spontaneous reaction between azo dyes ligands and metal ions under study is characterized by the negative value of (ΔG). The value of the gas constant (R)

Table 2. Stability constant and Gibbs free energy of the prepared complexes.

complexes	A_s	A_m	α	K	Lin k	$\Delta G \text{ kJ.mol}^{-1}$
[Ni(L) ₂]	0.063	0.154	0.590	8.20×10^6	15.919	-39.440
[Pd(L)Cl]	0.040	0.042	0.048	1.653×10^6	14.318	-35.474
[Pt(L) ₂]Cl ₂	0.087	0.206	0.577	9.0×10^6	16.013	-39.673



Scheme 7. Fragmentation pattern of Pd (II) complex.



Scheme 8. Fragmentation pattern of Pt (IV) complex.

is $8.314 \text{ J} \cdot \text{mol}^{-1} \cdot \text{K}$, while the absolute temperature (T) is expressed in Kelvin.

3.7 Physical estates

The ligand dissolved in ethanol interacted with the metal ions dissolved in a buffer solution of pH 7, resulting in the formation of stable complexes [35]. The ratio of metal to ligand was 1:2, except for Pd (II) which had a ratio of 1:1. The elemental analysis and metal extraction from compounds indicated that the measured values corresponded with the values obtained through calculation. When the ligand and metal complexes were dissolved in dimethylsulphoxide at a concentration of 10^{-3} mol/L , their conductivity indicated a non-electrolytic nature, except for the platinum complex which exhibited electrolyte behavior at a ratio of 1:2, as shown in Table 3.

3.8 UV-Vis spectroscopy of synthesized compounds

UV-Vis spectra were measured for the synthesized compounds dissolved in ethanol (10^{-3} mol/L), with the ex-

ception of the data provided in Table 3. The UV-Visible spectrum of the azo ligand displayed prominent absorption peaks at 202 nm associated with ($\pi-\pi^*$) transitions [36], as well as a peak at 448 nm linked to electronic transitions ($n-\pi^*$). The Ni (II) complex displayed three peaks at 278, 382, and 512 nm, which were associated with intra-ligand transitions and ($M \rightarrow L$) charge transfer involving the electronic transition of type ${}^3A_{2g} \rightarrow {}^3T_{1g}(P)$ [37]. Additional peaks at 780 and 845 nm indicated electronic transitions of type ${}^3A_{2g} \rightarrow {}^3T_{1g}(F)$ and ${}^3A_{2g} \rightarrow {}^3T_{2g}(F)$, respectively. The magnetic moment of this complex was determined to be 2.92 B.M., indicating a close resemblance to an octahedral environment. The Pd (II) complex spectrum exhibited peaks at 312 and 460 nm, attributed to intra-ligand transitions and ($M \rightarrow L$) charge transfer, with an additional peak at 576 nm assigned to ${}^1A_{1g} \rightarrow {}^1B_{1g}$ transitions [38]. The Pt (IV) spectrum displayed peaks at 206 and 462 nm corresponding to intra-ligand transitions and ($M \rightarrow L$) charge transfer, along with a peak at 578 nm due to ${}^1T_{1g}(F) \rightarrow {}^1T_{1g}(P)$ transitions [39]. The UV-Vis spectra of both ligands and metal com-

Table 3. The data regarding the conditions of the synthesized compounds, UV-Visible spectroscopy, magnetic susceptibility, and conductance measurements.

compounds	optimum pH	optimum molar conc. $\times 10^{-4}$	M:L ratio	(λ_{max}) nm	ABS	ϵ_{max} ($L.mol^{-1}.cm^{-1}$)	Λ_m ($S.cm^2.mol^{-1}$) In DMSO	μ_{eff} (B.M)
Ligand(L)	-	-	-	202 448	0.872 0.135	872 135	-	-
[Ni(L) ₂]	7	2.5	1:2	278 382 512 780 845	0.327 0.108 0.087 0.029 0.012	327 108 87 29 12	15.42	2.92
[Pd(L)Cl]	7	2.5	1:1	312 460 576	0.229 0.735 0.078	229 735 78	13.50	Di
[Pt(L) ₂]Cl ₂	7	2.5	1:2	206 462 578	2.406 0.144 0.030	2406 144 30	75.38	Di

plexes are illustrated in Fig. 12.

3.9 FT-IR spectroscopy of synthesized compounds

The compilation of the FTIR spectra for both the azo ligand and its metal complexes has been conducted, and the outcomes have been visually presented in Fig. 13. A stretching vibration of the $\nu(OH)$ phenol group was observed in the ligand spectrum, manifesting as a broad band at 3329 cm^{-1} [40]. The lack of this band in the spectra of the produced compounds suggests that the phenol group underwent deprotonation upon binding with the metal ion [41]. The absence of notable changes in the band at 3267 cm^{-1} , assigned to the $\nu(NH)$ vibration, implies that coordination did not take place through this particular donating atom. The spectrum displayed peaks at 1654 cm^{-1} and 1531 cm^{-1} , which can be attributed to the vibrations of $\nu(C=O)$ and $\nu(N=N)$, respectively [42]. Upon complexation, a shift towards lower frequencies was observed in these bands, indicating coordination with the metal ion. The complexes exhibited peaks at $(1600-1577)\text{ cm}^{-1}$ attributed to the $\nu(C=C)$ vibration, and peaks at $(1465-1369)\text{ cm}^{-1}$ indicative of the bending vibration of the $\delta(CH_3)$ group [43]. The identification of

stretching frequency bands corresponding to metal-nitrogen coordination, as opposed to metal-oxygen coordination, was additionally confirmed through the observation of bands ranging from 540 to 432 cm^{-1} .

3.10 Atomic absorption spectroscopy of Pd (II) complex

Furthermore, to assess the concentration of Pd in the complex, we employed atomic absorption spectroscopy. Our investigations involved the utilization of a standard solution with varying concentrations, which revealed that each milligram of the complex contained 0.004 mmol of Pd. Additionally, we verified these findings using an ICP instrument, and the results demonstrated a satisfactory level of agreement.

3.11 Suzuki cross-coupling reaction in the presence of Pd (II) complex

The optimization of reaction parameters plays a crucial role in catalytic reactions. This includes optimizing the quantity of catalyst, temperature, and choice of solvent. For the op-

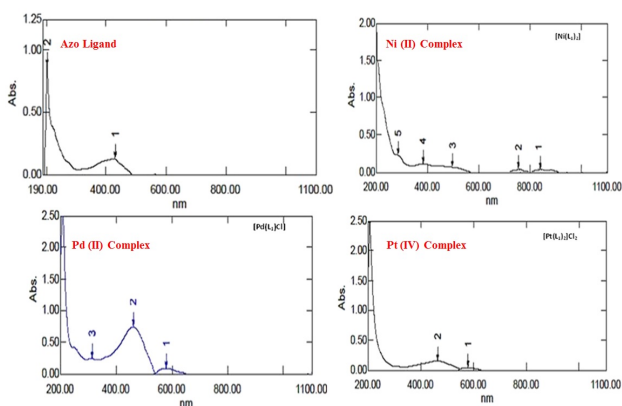


Figure 12. UV-Vis spectra of the synthesized compounds.

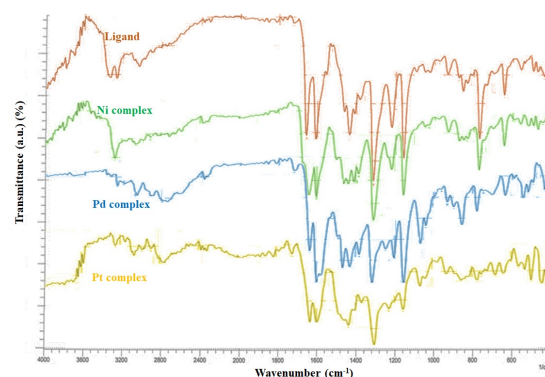


Figure 13. FT-IR spectroscopy of the synthesized compounds.

timization of reaction conditions in this research, the first step involved the selection of a model reaction. This model reaction comprised 1 mmol of 4-iodoanisole and 1.1 mmol of phenyl boronic acid, utilizing 1.5 mmol of base in 3 mL of solvent, with the presence of a Pd (II) complex. The details and results of this investigation are presented in Table 4. Various bases, such as Na₂CO₃, K₃PO₄, K₂CO₃, and Et₃N, were chosen to examine their impact on the model reaction (Table 4, entries 1-4). The experiments revealed that K₂CO₃ was the most suitable base for the model reaction (Table 4, entry 3). Furthermore, various solvents including water, ethanol, methanol, and acetonitrile were examined for the model reaction to determine their effects on the outcome (Table 4, entries 5-12). The ideal output for the model reaction when various solvents are present was achieved with a ratio of 2 parts H₂O to 1-part EtOH. Following the evaluation of the solvent effect on the model reaction, the catalyst amount and reaction temperature were analyzed (Table 4, entries 13-16). The optimal values for these parameters were found to be 20 mg of catalyst and 80 °C, as indicated by the results obtained.

After enhancing the reaction conditions, further investigation was conducted on various aryl halides using the refined parameters mentioned in Table 5. The efficacy of the Pd (II) complex has been observed in various aryl halides (X: Cl, Br, I) that possess both electron-donating and electron-withdrawing groups. Initially, the study focused on examining the responses of aryl iodides, which resulted in successful and satisfactory yields. However, when aryl bromides were utilized as substrates, the production of products yielded lower quantities. This decrease in yield can be attributed to the slower oxidation-addition process observed

in aryl bromides compared to aryl iodides. Furthermore, when aryl chloride was present, the reactivity was found to be inferior to that of its iodide and bromide counterparts.

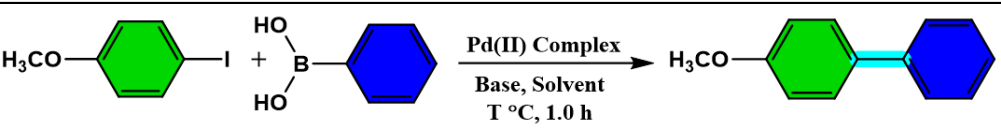
The reusability and recoverability of the Pd (II)-complex were also assessed during the synthesis of the target compound (Table 5, entry 1) with 4-iodoanisole as the initial aryl halide for a duration of 1 hour. After each trial, the reaction mixture was supplemented with 5.0 mL of hot water and 5.0 mL of ethyl acetate. The Pd-complex catalyst was acquired by applying reduced pressure through a sintered-glass apparatus using a vacuum pump. The findings indicate that the Pd (II)-complex maintained its catalytic activity after being recovered for four consecutive runs. The amount of leached Pd was quantified through ICP analysis. The presence of the azo ligand effectively hindered the release of Pd ions in significant quantities (Table 6).

3.12 Antimicrobial testing outcome

3.13 Effect of the synthesized compounds on Lymphatic Cell division in Human Blood

Fig. 14 illustrates the impact of Colchicine, ligand, and its complex on Lymphatic Cell during metaphase in human blood. The percentage of suspended cells halted in the metaphase of the ligand was recorded as 1.45, 1.57, and 2.34 at concentrations of 25, 50, and 100 µg/ml, respectively. In comparison, the control group exhibited a percentage of stopped cells at 4.62. Similarly, the percentage of suspended cells stopped in the metaphase of the platinum complex was observed as 0.90, 2.64, and 2.14 at concentrations of 25, 50, and 100 µg/ml, respectively, while the control group displayed a percentage of stopped cells at 4.33. Furthermore, the percentage of suspended

Table 4. Optimization Suzuki reaction^a.

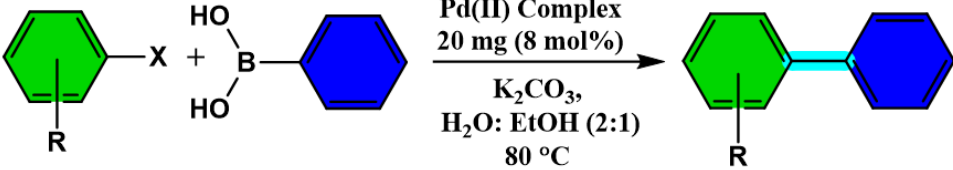


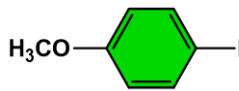
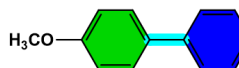
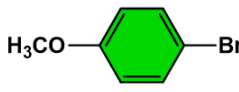
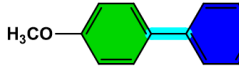
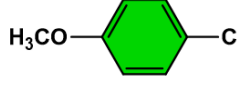
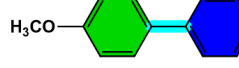
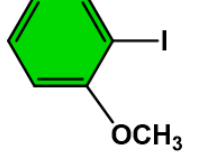

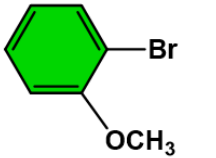
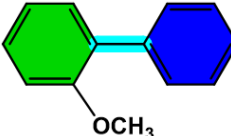
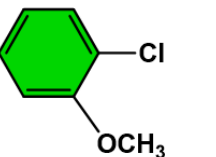
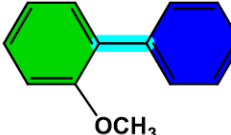
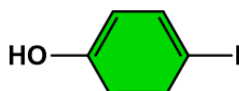
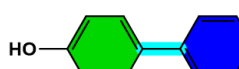

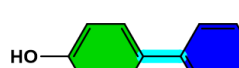

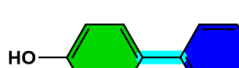






entry	base	solvent	catalyst (mg), (mol%)	T °C	yield (%) ^b
1	Na ₂ CO ₃	H ₂ O	20, 8	70	50
2	K ₃ PO ₄	H ₂ O	20, 8	70	45
3	K ₂ CO ₃	H ₂ O	20, 8	70	60
4	Et ₃ N	H ₂ O	20, 8	70	30
5	K ₂ CO ₃	EtOH	20, 8	70	50
6	K ₂ CO ₃	MeOH	20, 8	70	45
7	K ₂ CO ₃	CH ₃ CN	20, 8	65	55
8	K ₂ CO ₃	H ₂ O: EtOH (2:1)	20, 8	70	85
9	K ₂ CO ₃	H ₂ O: MeOH (2:1)	20, 8	70	75
10	K ₂ CO ₃	H ₂ O: CH ₃ CN (2:1)	20, 8	70	62
11	K ₂ CO ₃	H ₂ O: EtOH (1:1)	20, 8	70	80
12	K ₂ CO ₃	H ₂ O: EtOH (1:2)	20, 8	70	65
13	K ₂ CO ₃	H ₂ O: EtOH (2:1)	25, 10	70	85
14	K ₂ CO ₃	H ₂ O: EtOH (2:1)	15, 6	70	80
15	K ₂ CO ₃	H ₂ O: EtOH (2:1)	20, 8	80	96
16	K ₂ CO ₃	H ₂ O: EtOH (2:1)	20, 8	60	70

^a Reaction conditions: 1.0 mmol of 4-methoxyiodobenzene, 1.1 mmol of phenylboronic acid, 1.5 mmol of base, solvent: 3 mL.

^b Isolated yield (%).

Table 5. Scope of Suzuki reaction catalyzed Pd (II) complex^a.



entry	substrate	final product	time (h)	yield (%) ^b
1			1	96
2			1.3	94
3			2.0	90
4			1.6	93
5			2.0	93
6			3.2	88
7			1.1	97
8			1.8	96
9			2.3	89
10			2.1	91
11			2.5	85
12			3.1	79

^a Reaction conditions: 1.0 mmol of aryl halide; 1.1 mmol of phenyl boronic acid; 1.5 mmol of K₂CO₃; solvent (3 mL); T: 80 °C. catalyst 8.0 mol% b) Isolated Yield (%).

Table 6. The reusability and recoverability of Pd (II)-complex in Suzuki coupling reaction.

entry	yield (%) ^a	Pd-leached (%) ^b	time (h)
1	96%	2.5%	1
2	91%	1.3%	1
3	88%	1.2%	1
4	86%	1.6%	1

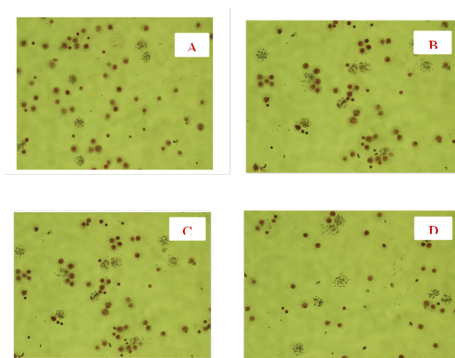
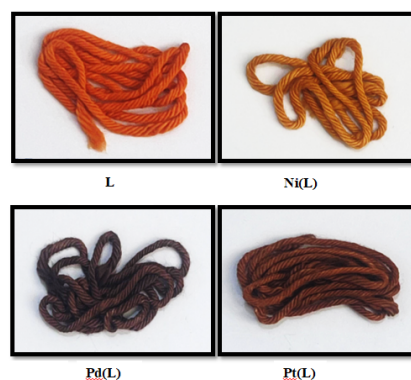
^a Isolated yield.^b Determined by atomic absorption for entry 1 and other entries determined by ICP.

cells stopped in the metaphase of the palladium complex was measured as 1.81, 2.67, and 3.97 at concentrations of 25, 50, and 100 $\mu\text{g/ml}$, respectively, with the control group exhibiting a percentage of stopped cells at 4.10 as shown in Table 7. The results suggest that the ligand and its complexes influence the proliferation of lymphocytes, showing the least inhibition rate of $1.45 \text{ b} \pm 0.11$ at 25 mg/mL concentration and the highest inhibition rate of $2.34 \text{ c} \pm 0.03$ at 100 Mg/ml concentration for L. In the case of the Pd complex and lymphocytes proliferation cell line, the lowest inhibition rate was measured as $1.81 \text{ b} \pm 0.13$ at a concentration of 25 Mg/ml , while the highest inhibition rate was recorded as

$3.97 \text{ d} \pm 0.02$ at a concentration of 100 Mg/ml . These results suggest that the palladium complex possesses the ability to halt lymphocyte division during the tropic phase through its influence on microtubules and spindle filaments.

3.14 Performance of dyeing

The effectiveness of the chemical dyes in coloring cotton fabrics has already been established. The colors play a crucial role in enhancing the brightness and stability of the detergent. As a result, complete dyes demonstrate exceptional dyeing stability and offer a rich texture. The illustration of the coloring process can be observed in Fig. 15.

**Figure 14.** Human lymphocytes in metaphase treatment with (A) Colchicine, (B)L, (C) $[\text{Pt}(\text{L})_2]\text{Cl}_2$, (D) $[\text{Pd}(\text{L})]\text{Cl}$ in concentration 100 mg/mL .**Figure 15.** Textiles dyeing by azo ligand (L) and its complexes.**Table 7.** Study the effect of (L1, L1pt, L1pd) in Mitotic Index (chromosome) in lymphocytes of humans.

	L1	L1pt	L1pd
concentration ($\mu\text{g/ml}$)	the percentage of cells in the tropical phase inhibition \pm standard deviation	the percentage of cells in the tropical phase inhibition \pm standard deviation	the percentage of cells in the tropical phase standard deviation \pm inhibition
control (cholgsen)	$4.62 \text{ a} \pm 0.01$	$4.33 \text{ a} \pm 0.11$	$4.10 \text{ a} \pm 0.01$
25	$1.45 \text{ b} \pm 0.11$	$0.90 \text{ b} \pm 0.11$	$1.81 \text{ b} \pm 0.13$
50	$1.57 \text{ b} \pm 0.10$	$2.64 \text{ c} \pm 0.12$	$2.67 \text{ c} \pm 0.12$
100	$2.34 \text{ c} \pm 0.03$	$2.14 \text{ c} \pm 0.03$	$3.97 \text{ d} \pm 0.02$

4. Conclusions

In this study, we have presented the synthesis and spectral analysis of a novel azo dye ligand obtained from 5-amino-2,3-dihydrophthalazine-1,4-dione and 3,5-dimethylphenol. The azo ligand was characterized using various spectroscopic techniques such as FTIR, UV-Vis, ^1H and ^{13}C NMR, Mass spectrometry, as well as micro elemental analysis (C, H, N, O). Furthermore, metal complexes of the ligand with Ni (II), Pd (II), and Pt (IV) ions were prepared and analyzed. A variety of metal complexes were prepared and examined through elemental analysis, infrared and UV-Vis's spectroscopy, mass spectrometry, conductivity measurements, and magnetic investigations. The analytical data indicated that most complexes exhibited a 1:2 metal-ligand ratio, with the exception of the palladium complex which displayed a 1:1 ratio. Based on physicochemical data, an octahedral structure was proposed for the Ni (II) and Pt (IV) complexes, while a square planar geometry was suggested for the Pd (II) complex. Additionally, the Pd (II) complex was utilized in a Suzuki cross-coupling reaction. Moreover, the impact of the complexes on blood lymphocyte division in the presence of PHA was investigated. The results revealed that the ligand (L1) hindered cell division to varying degrees, with the inhibitory effect increasing with higher concentrations. Moreover, the Pd coordination compound obstructed the proliferation of lymphocytes by triggering a persistent arrest in mitosis at the metaphase/anaphase boundary.

Authors Contributions

Authors have equal contribution role in preparing the paper.

Availability of Data and Materials

The data that support the findings of this study are available from the corresponding author upon reasonable request.

Conflict of Interests

The authors declare that they have no known competing financial interests or personal relationships that could have appeared to influence the work reported in this paper.

Open Access

This article is licensed under a Creative Commons Attribution 4.0 International License, which permits use, sharing, adaptation, distribution and reproduction in any medium or format, as long as you give appropriate credit to the original author(s) and the source, provide a link to the Creative Commons license, and indicate if changes were made. The images or other third party material in this article are included in the article's Creative Commons license, unless indicated otherwise in a credit line to the material. If material is not

included in the article's Creative Commons license and your intended use is not permitted by statutory regulation or exceeds the permitted use, you will need to obtain permission directly from the OICC Press publisher. To view a copy of this license, visit <https://creativecommons.org/licenses/by/4.0>.

References

- [1] V. Vidya and V. Sadasivan. Synthesis, spectroscopic characterization and biological activities of some metal complexes with new heterocyclic azodye ligand 2-(2-hydroxynaphthalen-1-yl azo)-pyridin-3-ol. *Curr. Chem. Lett.*, **12**(2023):55–64. DOI: <https://doi.org/10.5267/j.ccl.2022.9.006>.
- [2] B. Derkowska-Zielinska, E. Gondek, M. Pokladko-Kowar, A. Kaczmarek-Kedziera, A. Kysil, G. Lakshminarayana, and O. Krupka. Photovoltaic cells with various azo dyes as components of the active layer. *Solar Energy*, **203**(2020):19–24, . DOI: <https://doi.org/10.1016/j.solener.2020.04.022>.
- [3] B. Derkowska-Zielinska, K. Matczyszyn, M. Dudek, M. Samoc, R. Czaplicki, A. Kaczmarek-Kedziera, V. Smokal, A. Biitseva, and O. Krupka. All-optical poling and two-photon absorption in heterocyclic azo dyes with different side groups. *The Journal of Physical Chemistry C*, **123**(2019):725–734, . DOI: <https://doi.org/10.1021/acs.jpcc.8b10621>.
- [4] B. Derkowska-Zielinska, D. Szmigiel, A. Kysil, O. Krupka, and A. Kozanecka-Szmigiel. Photoreponsive behavior of heterocyclic azo polymers with various functional groups. *The Journal of Physical Chemistry C*, **124**(2020):939–944, . DOI: <https://doi.org/10.1021/acs.jpcc.9b10495>.
- [5] N.A. El-Wakiel. Synthesis and characterization of azo sulfaguanidine complexes and their application for corrosion inhibition of silicate glass. *Appl. Organomet. Chem.*, **30**(2016):664–673. DOI: <https://doi.org/10.1002/aoc.3487>.
- [6] P.B. Raja, M. Ismail, S. Ghoreishiamiri, J. Mirza, M.C. Ismail, S. Kakooei, and A.A. Rahim. Reviews on corrosion inhibitors: A short view. *Chem. Eng. Commun.*, **203**(2016):1145–1156. DOI: <https://doi.org/10.1080/00986445.2016.1172485>.
- [7] N. Ranjitha, G. Krishnamurthy, M.N. Manjunatha, H.S.B. Naik, M. Pari, V.N. K, J. Lakshmikantha, and K. Pradeepa. Electrochemical determination of glucose and H_2O_2 using Co(II), Ni(II), Cu(II) complexes of novel 2-(1,3-benzothiazol-2-ylamino)-N-(5-chloro-2-hydroxyphenyl)acetamide: Synthesis, structural characterisation, antimicrobial, anticancer activity and docking studies. *J. Mol. Struct.*, **1274**(2023):134483. DOI: <https://doi.org/10.1016/j.molstruc.2022.134483>.

- [8] M. Gaber, S.K. Fathalla, and H.A. El-Ghamry. 2,4-Dihydroxy-5-[(5-mercapto-1H-1,2,4-triazole-3-yl)diazanyl]benzaldehyde acetato, chloro and nitrate Cu(II) complexes: Synthesis, structural characterization, DNA binding and anticancer and antimicrobial activity. *Appl. Organomet. Chem*, **33**(2019):e4707. DOI: <https://doi.org/10.1002/aoc.4707>.
- [9] A.M. Al-Etaibi and M.A. El-Asasery. A comprehensive review on the synthesis and versatile applications of biologically active pyridone-based disperse dyes. *International Journal of Environmental Research and Public Health*, **17**(2020):4714.
- [10] A.R.E. Mahdy, O.A. Abu Ali, W.M. Serag, E. Fayad, R.F.M. Elshaarawy, and E.M. Gad. Synthesis, characterization, and biological activity of Co(II) and Zn(II) complexes of imidazoles-based azo-functionalized Schiff bases. *J. Mol. Struct.*, **1259**(2022):132726. DOI: <https://doi.org/10.1016/j.molstruc.2022.132726>.
- [11] H.A.K. Kyhoiesh and K.J. Al-Adilee. Synthesis, spectral characterization, antimicrobial evaluation studies and cytotoxic activity of some transition metal complexes with tridentate (N,N,O) donor azo dye ligand. *Results in Chemistry*, **3**(2021):100245. DOI: <https://doi.org/10.1016/j.rechem.2021.100245>.
- [12] H.S. Mandour, S.A. Abouel-Enein, R.M.M. Morsi, and L.A. Khorshed. Azo ligand as new corrosion inhibitor for copper metal: Spectral, thermal studies and electrical conductivity of its novel transition metal complexes. *J. Mol. Struct.*, **1225**(2021):129159. DOI: <https://doi.org/10.1016/j.molstruc.2020.129159>.
- [13] J.M.M. Al-Zinkee and A.J. Jarad. Synthesis, spectral studies and microbial evaluation of azo dye ligand complexes with some transition metals. *Journal of Pharmaceutical Sciences and Research*, **11**(2019):98–103.
- [14] L. Song, L. Cai, L. Gong, and E.V. Van der Eycken. Photoinduced copper-catalyzed enantioselective coupling reactions. *Chem. Soc. Rev.*, **52**(2023):2358–2376. DOI: <https://doi.org/10.1039/D2CS00734G>.
- [15] M. Ashraf, M.S. Ahmad, Y. Inomata, N. Ullah, M.N. Tahir, and T. Kida. Transition metal nanoparticles as nanocatalysts for Suzuki, Heck and Sonogashira cross-coupling reactions. *Coord. Chem. Rev.*, **476**(2023):214928. DOI: <https://doi.org/10.1016/j.ccr.2022.214928>.
- [16] M.H. Samha, L.J. Karas, D.B. Vogt, E.C. Odogwu, J. Elward, J.M. Crawford, J.E. Steves, and M.S. Sigman. Predicting success in Cu-catalyzed C–N coupling reactions using data science. *Science Advances*, **10**(2024):eadn3478. DOI: <https://doi.org/10.1126/sciadv.adn3478>.
- [17] D.P. Patel and S. Kumar Singh. Rose-Bengal-Photocatalyzed cross-dehydrogenative coupling reactions under visible light. *Eur. J. Org. Chem.*, **27**(2024):e202301185. DOI: <https://doi.org/10.1002/ejoc.202301185>.
- [18] P. Onnuch, K. Ramagonolla, and R.Y. Liu. Aminative Suzuki–Miyaura coupling. *Science*, **383**(2024):1019–1024. DOI: <https://doi.org/10.1126/science.adl5359>.
- [19] S.A. Jacoby, N.W. Harris, A. Wiemann, C.D. Glenn, A.R. Kantzler, L.P. Dinh, and L. Yet. Suzuki–Miyaura and Buchwald–Hartwig cross-coupling reactions utilizing a set of complementary imidazopyridine monophosphine ligands. *ChemistrySelect*, **9**(2024):e202305085. DOI: <https://doi.org/10.1002/slct.202305085>.
- [20] K. Goswami, D. Das, P. Bera, S. Roy, M.M. Seikh, P.K. Sinha, and A. Gayen. One-pot synthesis of ligand-free highly active Pd catalyst supported on NiFe spinel oxide for Suzuki–Miyaura cross-coupling reaction. *J. Mol. Struct.*, **1299**(2024):137136. DOI: <https://doi.org/10.1016/j.molstruc.2023.137136>.
- [21] B. Karimi, F. Mansouri, and H.M. Mirzaei. Recent applications of magnetically recoverable nanocatalysts in C–C and C–X Coupling Reactions. *ChemCatChem*, **7**(2015):1736–1789. DOI: <https://doi.org/10.1002/cctc.201403057>.
- [22] B. Karimi, F. Mansouri, and H. Vali. A highly water-dispersible/magnetically separable palladium catalyst based on a Fe₃O₄@SiO₂ anchored TEG-imidazolium ionic liquid for the Suzuki–Miyaura coupling reaction in water. *Green Chem.*, **16**(2014):2587–2596. DOI: <https://doi.org/10.1039/C3GC42311E>.
- [23] P. Gao and M. Szostak. Hydration reactions catalyzed by transition metal–NHC (NHC = N-heterocyclic carbene) complexes. *Coord. Chem. Rev.*, **485**(2023):215110. DOI: <https://doi.org/10.1016/j.ccr.2023.215110>.
- [24] T. Aziz, H.A. Nasim, K. Ahmad, H. u. R. Shah, S. Parveen, M.M. Ahmad, H. Majeed, A.M. Galal, A. Rauf, and M. Ashfaq. Rational synthesis, biological screening of azo derivatives of chloro-phenylcarbonyl diazenyl hydroxy dipyrimidines/thioxotetrahydropyrimidines and their metal complexes. *Heliyon*, **9**(2023):e12492. DOI: <https://doi.org/10.1016/j.heliyon.2022.e12492>.
- [25] F. Al-Haj Hussien. An eco-friendly methodology for the synthesis of azocoumarin dye using cation exchange resins. *Heliyon*, **7**(2021):e08439. URL [10.1016/j.heliyon.2021.e08439](https://doi.org/10.1016/j.heliyon.2021.e08439).
- [26] B.G. Devika, B.H. Doreswamy, N.M. Mallikarjuna, and H.C. Tandon. Synthesis, characterisation and molecular structure study of metal complexes of antipyrine based ligand. *J. Mol. Struct.*, **1185**(2019):69–77. DOI: <https://doi.org/10.1016/j.molstruc.2019.02.029>.

- [27] N.M. Mallikarjuna, J. Keshavayya, M.R. Maliyappa, R.A. Shoukat Ali, and T. Venkatesh. Synthesis, characterization, thermal and biological evaluation of Cu (II), Co (II) and Ni (II) complexes of azo dye ligand containing sulfamethaxazole moiety. *J. Mol. Struct.*, **1165**(2018):28–36. DOI: <https://doi.org/10.1016/j.molstruc.2018.03.094>.
- [28] R.S. Verma and A. Babu. Book: Human chromosomes: manual of basic techniques. , 1989.
- [29] R. Carballo, A. Castiñeiras, B. Covelo, J. Niclós, and E.M. Vázquez-López. Synthesis and characterization of a potassium complex of magnesium: $[K(HL)(OH_2)_2]_{\infty}$ [H₂L=4-(4-nitrophenylazo)resorcinol (magneson)]. *Polyhedron*, **20**(2001):2415–2420. DOI: [https://doi.org/10.1016/S0277-5387\(01\)00842-7](https://doi.org/10.1016/S0277-5387(01)00842-7).
- [30] R.H. Fayadh, A.A. Ali, and F.M. Al-Jabri. Synthesis and identification symmetrically azo dyes derived from sulfa compounds and spectrophotometric study of nickel (II) complexes with prepared dyes. *International Journal of Engineering and Technical Research (IJETR)*, **3**(2015):25–28.
- [31] A. Skotnicka and P. Czeleń. Substituent and solvent polarity on the spectroscopic properties in Azo derivatives of 2-hydroxynaphthalene and their difluoroboranes complexes. *Materials*, **14**(2021):3387.
- [32] R. Khanum, R.A. Shoukat Ali, H.R. Rangaswamy, S.R. Santhosh Kumar, A.G. Prashantha, and A.S. Jagadisha. Recent review on synthesis, spectral studies, versatile applications of azo dyes and its metal complexes. *Results in Chemistry*, **5**(2023):100890. DOI: <https://doi.org/10.1016/j.rechem.2023.100890>.
- [33] E. Williams and N. Bartelt. Book: Thermodynamics and statistical. , 1996.
- [34] W.J. Geary. The use of conductivity measurements in organic solvents for the characterisation of coordination compounds. *Coord. Chem. Rev.*, **7**(1971):81–122. DOI: [https://doi.org/10.1016/S0010-8545\(00\)80009-0](https://doi.org/10.1016/S0010-8545(00)80009-0).
- [35] A.J. Jarad, M.A. Dahi, T.H. Al-Noor, M.M. El-ajaily, S.R. Al-Ayash, and A. Abdou. Synthesis, spectral studies, DFT, biological evaluation, molecular docking and dyeing performance of 1-(4-((2-amino-5-methoxy)diazenyl)phenyl) ethanone complexes with some metallic ions. *J. Mol. Struct.*, **1287**(2023):135703, . DOI: <https://doi.org/10.1016/j.molstruc.2023.135703>.
- [36] M.H. Keshavarz, Z. Shirazi, A. Barghahi, A. Mousavi-azar, and A. Zali. A novel model for prediction of stability constants of the thiosemicarbazone ligands with different types of toxic heavy metal ions using structural parameters and multivariate linear regression method. *Environmental Science and Pollution Research*, **29**(2022):37084–37095. DOI: <https://doi.org/10.1007/s11356-021-17714-w>.
- [37] I.N. Witwit, H.M. Farhan, and Z.Y. Motaweq. Preparation of mixed ligand complexes of heterocyclic Azo quinoline ligand and imidazole molecule with some of divalent transition ions and their biological activity against multi drug resistance pathogenic bacteria. *Journal of Physics: Conference Series*, **1879**(2021):022064. DOI: <https://doi.org/10.1088/1742-6596/1879/2/022064>.
- [38] M.Q. Abdulridha, A.A.S. Al-Hamdani, and W. Al Zoubi. Synthesis, spectral identification, thermal and antioxidant studies for Ni (II), Pd (II), Pt (IV) and Au (III) complexes with new Azo ligand derivatives from tryptamine. *Ibn AL-Haitham Journal For Pure and Applied Sciences*, **36**(2023):303–320. DOI: <https://doi.org/10.30526/36.4.3059>.
- [39] N. Abbas. Synthesis, characterization and applications of mono Azo, oo metal complex dyes of Cr (III), Fe (II), Co (II) and Cu (II). *Sch Int J Chem Mater Sci*, **4**(2021):127–140. DOI: <https://doi.org/10.36348/sijcms.2021.v04i06.002>.
- [40] K.J. Al-adilee, B.A. Hatem, and O.A. Hatem. Synthesis and spectral characterization of new azo dye derived from benzimidazole and its complexation with selected transition metal ions. *Journal of Physics: Conference Series*, **1999**(2021):012123. DOI: <https://doi.org/10.1088/1742-6596/1999/1/012123>.
- [41] A.J. Jarad, I.Y. Majeed, and A.O. Hussein. Synthesis and spectral studies of heterocyclic azo dye complexes with some transition metals. *Journal of Physics: Conference Series*, **1003**(2018):012021, . DOI: <https://doi.org/10.1088/1742-6596/1003/1/012021>.
- [42] R. Sharma, P. Giri, D.K.D. Kumar, and N. Neelam. Synthesis, spectral and antimicrobial activity of mixed ligand complexes of Co(II), Ni(II), Cu(II) and Zn(II) with N,O and S donor ligands. *Journal of Chemical and Pharmaceutical Research*, **4**:1969–1973.
- [43] K. Mostafa MH, I. Eman H, M. Gehad G, Z. Ehab M, and B. Ahmed. Synthesis and characterization of a novel schiff base metal complexes and their application in determination of iron in different types of natural water. *Open Journal of Inorganic Chemistry*, **2012**(2012):1–9. DOI: <https://doi.org/10.4236/ojic.2012.22003>.